Inelastic Neutrino-Helium Scatterings and Standing Accretion Shock Instability in Core-Collapse Supernovae

Naofumi Ohnishi[1], Kei Kotake[2], and Shoichi Yamada[3,4]

[1]*Department of Aerospace Engineering, Tohoku University, 6-6-01 Aramaki-Aza-Aoba, Aoba-ku, Sendai, 980-8579, Japan*

ohnishi@cfd.mech.tohoku.ac.jp

[2] *National Astronomical Observatory of Japan, 2-21-1, Osawa, Mitaka, Tokyo, 181-8588, Japan*

kkotake@th.nao.ac.jp

[3]*Science & Engineering, Waseda University, 3-4-1 Okubo, Shinjuku, Tokyo, 169-8555, Japan*

shoichi@heap.phys.waseda.ac.jp

[4]*Advanced Research Institute for Science and Engineering, Waseda University, 3-4-1 Okubo, Shinjuku, Tokyo, 169-8555, Japan*

shoichi@heap.phys.waseda.ac.jp

ABSTRACT

We present the results of numerical experiments, in which we have investigated the influence of the inelastic neutrino-helium interactions on the standing accretion shock instability supposed to occur in the post-bounce supernova core. The axisymmetric hydrodynamical simulations of accretion flows through the standing accretion shock wave onto the protoneutron star show that the interactions are relatively minor and the linear growth of the shock instability is hardly affected. The extra heating given by the inelastic reactions becomes important for the shock revival after the instability enters the non-linear regime, but only when the neutrino luminosity is very close to the critical value, at which the shock would be revived without the interactions. We have also studied the dependence of the results on the initial amplitudes of perturbation and the temperatures of mu and tau neutrinos.

Subject headings: supernovae: general — neutrinos — hydrodynamics — instabilities

1. Introduction

Most of the supernova modelers are currently concerned with the multi-dimensional aspects of the dynamics, pushed by the accumulating observational evidences that the core-collapse supernovae are generally aspherical (Wang et al. 1996, 2001, 2002). Various mechanisms to produce the asymmetry have been considered so far. Among them are the convection (e.g., Herant et al. (1994); Burrows et al. (1995); Janka & Mueller (1996)), growth of asymmetry seed generated prior to core-collapse (Burrows & Hayes 1996; Fryer 2004), rotation and magnetic fields (see Yamada & Sawai (2004); Kotake et al. (2004); Takiwaki et al. (2004); Sawai et al. (2005); Ardeljan et al. (2005) and Kotake et al. (2006) for collective references).

Recently the standing accretion shock instability (SASI) is attracting interest of researchers. The instability was originally studied for transonic accretion flows to black holes (e.g., Foglizzo (2001, 2002)) and was re-discovered by Blondin et al. (2003) in the context of core-collapse supernovae. Blondin et al. (2003) found in their 2D numerical simulations of the spherically symmetric, isentropic, steady accretion flows, that a standing shock wave are unstable to non-spherical perturbations and that the perturbations grow up to the nonlinear regime with the clear dominance of the $\ell = 1$ mode at first and $\ell = 2$ mode later, leading to the global deformation of the shock wave as has been observed. Here ℓ stands for the azimuthal index of the Legendre polynomials.

The mechanism of the instability is still controversial. Blondin & Mezzacappa (2006) took coolings into account in a simple analytic way following Houck & Chevalier (1992) and claimed that the repeated propagations of pressure fluctuations are responsible for the instability. On the other hand, Ohnishi et al. (2006) did 2D numerical experiments, implementing more realistic heatings as well as coolings by neutrino and found that the original idea by Foglizzo (2001, 2002) that the non-radial instability is driven by the cycle of the advection of entropy and velocity fluctuations and propagation of pressure perturbations seems to be more appropriate. Obviously detailed linear analyses of the instability are needed (Galletti & Foglizzo 2005; Yamasaki & Yamada 2006b).

It is important that such a low-ℓ-mode deformation of the shock wave has been also observed in more realistic simulations (Scheck et al. 2004) and that the asymmetric explosion following the instability might reproduce various non-spherical features of SN1987A (Kifonidis et al. 2005). It should be also emphasized that the instability is helpful for the shock revival just as the convection is (Ohnishi et al. 2006). The problem is whether the instability enhances the neutrino heating sufficiently to revive the stalled shock. Recent numerical investigations by Janka et al. (2005) seem to say "no" to this question. It is true that we have to wait for detailed 3D simulations before drawing a conclusion, but we had better

continue to seek for some other processes that would further facilitate the shock revival. As such a potential boost, we will focus in this paper on the interplay between the inelastic neutrino-nucleus interactions and the SASI.

The potential importance of the inelastic neutrino-nucleus interactions was first pointed out by Haxton (1988), who paid attention to the heating and dissociations of nuclei in the matter ahead of the shock wave via these reactions, the so-called preheating. Taking the reactions into account in their 1D spherically symmetric numerical simulations, Bruenn & Haxton (1991) found that the effect of preheating is quite minor mainly because ν_e energies obtained in the simulation was lower than the one assumed in Haxton (1988). They also discussed the possibility of shock revival by enhanced heating of the postshock material by inelastic $\nu_{\tau,\mu} - {}^4$He scatterings, the idea similar to ours pursued in this paper. They found that the reactions are not very important. It should be emphasized, however, that the conclusion will be sensitive to the background model and they considered a single snapshot after the bounce. Furthermore, in the spherically symmetric models, most of the nuclei are photodisintegrated after passing through the shock and the reactions will scarcely occur anyway. The situation may be different in non-spherical cases. Since the shock wave hovers at larger radius in general, not all the nuclei are dissociated and the heating region will be wider. In this paper, we pay particular attention to the interplay between the SASI and the inelastic reactions.

The plan of this paper is as follows. We describe the numerical methods, input physics and models in section 2. The main numerical results are shown in section 3. We conclude this paper with section 4.

2. Numerical Method, Input Microphysics and Models

In this paper we study the effect of the inelastic neutrino-helium interactions on the evolution of accretion flows through a shock wave onto a protoneutron star, in particular the growth of SASI. We assume the axisymmetry of the system and do 2D numerical simulations.

The numerical methods employed in this paper are essentially the same as those used in our previous paper (Ohnishi et al. 2006). The following equations describe the compressible accretion flows of matter attracted by the protoneutron star and irradiated by neutrinos emitted from the neutrino sphere.

$$\frac{d\rho}{dt} + \rho \nabla \cdot \boldsymbol{v} = 0, \tag{1}$$

$$\rho \frac{d\boldsymbol{v}}{dt} = -\nabla P - \rho \nabla \Phi, \tag{2}$$

$$\rho\frac{d}{dt}\left(\frac{e}{\rho}\right) = -P\nabla \cdot \boldsymbol{v} + Q_{\text{E}} + Q_{\text{inel}}, \tag{3}$$

$$\frac{dY_{\text{e}}}{dt} = Q_{\text{N}}, \tag{4}$$

$$\Phi = -\frac{GM_{\text{in}}}{r}, \tag{5}$$

where ρ, $\boldsymbol{v}$, e, P, Y_{e}, and Φ are density, velocity, internal energy, pressure, electron fraction, and gravitational potential, respectively. We denote the Lagrangian derivative as d/dt and r is the radius. The self-gravity of matter in the accretion flow is ignored (see Yamasaki & Yamada (2006a) for the effect). The parameters of Q_{E} and Q_{N} are related with the interactions of neutrinos and free nucleons (see also Ohnishi et al. (2006)). M_{in} is the mass of the central object.

In addition to the standard heating and cooling via neutrino absorptions and emissions by free nucleons, here we consider the inelastic neutrino-helium interactions. The heating rates denoted as Q_{inel} were estimated by Haxton (1988) for the inelastic scatterings on nuclei via neutral currents, $\nu + (A, Z) \rightarrow \nu + (A, Z)^*$, as follows,

$$
\begin{aligned}
Q_{\text{inel}} = \frac{\rho X_{\text{A}}}{m_{\text{B}}}\frac{31.6\text{MeV}}{(r/10^7\text{cm})^2} & \left[\frac{L_{\nu_{\text{e}}}}{10^{52}\text{ergs s}^{-1}}\left(\frac{5\text{MeV}}{T_{\nu_{\text{e}}}}\right)\frac{A^{-1}\langle\sigma_{\nu_{\text{e}}}^+ E_{\nu_{\text{e}}} + \sigma_{\nu_{\text{e}}}^0 E_{\text{ex}}^{\text{A}}\rangle_{T_{\nu_{\text{e}}}}}{10^{-40}\text{cm}^2\text{MeV}}\right. \\
& + \frac{L_{\bar{\nu}_{\text{e}}}}{10^{52}\text{ergs s}^{-1}}\left(\frac{5\text{MeV}}{T_{\bar{\nu}_{\text{e}}}}\right)\frac{A^{-1}\langle\sigma_{\bar{\nu}_{\text{e}}}^- E_{\nu_{\text{e}}} + \sigma_{\bar{\nu}_{\text{e}}}^0 E_{\text{ex}}^{\text{A}}\rangle_{T_{\bar{\nu}_{\text{e}}}}}{10^{-40}\text{cm}^2\text{MeV}} \\
& \left. + \frac{L_{\nu_{\mu}}}{10^{52}\text{ergs s}^{-1}}\left(\frac{10\text{MeV}}{T_{\nu_{\mu}}}\right)\frac{A^{-1}\langle\sigma_{\nu_{\mu}}^0 E_{\text{ex}}^{\text{A}} + \sigma_{\bar{\nu}_{\mu}}^0 E_{\text{ex}}^{\text{A}}\rangle_{T_{\nu_{\mu}}}}{10^{-40}\text{cm}^2\text{MeV}}\right], \tag{6}
\end{aligned}
$$

where X_{A} is the mass fraction of the nucleus and m_{B} is the atomic mass unit. L_ν and T_ν in the square brackets are the neutrino luminosity and temperature, respectively, and A is the mass number of the nucleus. The last term denotes the sum of the contributions from mu and tau neutrinos. The cross section for each neutral-current is evaluated by the following fitting formula,

$$A^{-1}\langle\sigma_\nu^0 E_{\text{ex}}^{\text{A}} + \sigma_{\bar{\nu}}^0 E_{\text{ex}}^{\text{A}}\rangle_{T_\nu} = \alpha\left[\frac{T_\nu - T_0}{10\text{MeV}}\right]^\beta, \tag{7}$$

where α, β, and T_0 are given in Table I of Haxton (1988). Since we are concerned with the reactions with ^{4}He, the only nucleus that is abundant in the post shock matter, these parameters are chosen to be $\alpha = 1.24\times 10^{-40}$ MeV cm^2, $\beta = 3.82$, and $T_0 = 2.54$ MeV. In the first and second terms on the right hand side of Eq. (6), the contributions from the charged current reactions, σ_ν^+ and σ_ν^-, are also taken into account according to Table II of Haxton (1988). We ignore the variations of the electron fraction by these reactions, since they are minor and give no qualitative difference to the dynamics. Considering the uncertainties

inherent to the theoretical estimation of the reaction rates, we multiply rather arbitrarily the rates obtained above and discuss the dependence of the outcomes on this factor.

The numerical code employed in this paper is based on the ZEUS-2D (Stone & Norman 1992), which is an Eulerian code based on the finite-difference method with an artificial viscosity of von Neumann and Richtmyer type. We have made several major changes to the base code to include appropriate microphysics. For example, we have added the equation for electron fraction (Eq. (4)), which is solved in the operator-splitting fashion. We have also incorporated the tabulated realistic equation of state (EOS) based on the relativistic mean field theory (Shen et al. 1998) instead of the ideal gas EOS assumed in the original code. The reason why only ^{4}He is considered in this paper is that the abundance of other nuclei is negligibly small in the post-shock matter. The mass fraction of ^{4}He is obtained from the EOS.

Spherical coordinates are used. No equatorial symmetry is assumed and the computation domain covers the whole meridian section with 60 angular mesh points, except for a model in which we have adopted 120 angular mesh points. Since the latter model did not produce any significant difference from other models, we will report in the following the results obtained from the models with 60 angular mesh points. We use 300 radial mesh points to cover $r_{\mathrm{in}} \leq r \leq r_{\mathrm{out}} = 2000$ km, where r_{in} is the inner boundary and chosen to be roughly the radius of neutrino sphere.

The initial conditions are prepared in the same manner as in Ohnishi et al. (2006). The steady state solutions obtained by Yamasaki & Yamada (2005) for a fixed density at the inner boundary, $\rho_{\mathrm{in}} = 10^{11}$ g cm^{-3}, are utilized. In so doing, Q_{inel} is not taken into account. Hence the initial state is not completely steady when the inelastic interactions are considered and this slight inconsistency can be regarded as an additional radial perturbation. As shown shortly, however, the effect is small and limited to a very narrow region, and matters little to the analysis of the following dynamics. To induce the non-spherical instability, we have added $\ell = 1$ velocity perturbations to the initial state mentioned above.

All the numerical models are summarized in Table 1. The mass accretion rate and the mass of protoneutron star are fixed to be $\dot{M} = 1\ M_\odot$ s^{-1} and $M_{\mathrm{in}} = 1.4\ M_\odot$, respectively. The temperatures of electron-type neutrinos are also constant and set to be $T_{\nu_{\mathrm{e}}} = 4$ MeV and $T_{\bar{\nu}_{\mathrm{e}}} = 5$ MeV, which are the typical values in the post-bounce phase. For most of the models, the temperature of mu and tau neutrinos is chosen to be $T_{\nu_\mu} = 10$ MeV, but we also vary it to investigate the dependence of the dynamics on this parameter. Note that the reaction rates are very sensitive to the incident energy of neutrino (see Eq. (7)). The neutrino luminosity is also varied in this study. In the reference model, the luminosity of electron-type neutrino $L_{\nu_{\mathrm{e}}}$ and anti-neutrino $L_{\bar{\nu}_{\mathrm{e}}}$ are set to be 5.9×10^{52} ergs s^{-1}. It is

noted that this value is very close to the threshold, $L_{\nu_e,\bar{\nu}_e} = 6.0 \times 10^{52}$ ergs s^{-1}, at which a SASI-triggered shock revival occurs without inelastic interactions as described in Ohnishi et al. (2006). The luminosity of mu and tau neutrinos is set to be half that of electron-type neutrinos according to the results obtained by detailed simulations (e.g., Liebendörfer et al. (2001)).

3. Results

Figure 1 shows the mass fractions of proton, neutron and helium (upper panel) and the profiles of $Q_{\rm E}$ and $Q_{\rm inel}$ (lower panel) at the initial time for the reference model L59I0, where L_{ν_e} is set to be 5.9×10^{52} ergs s^{-1} and $T_{\nu_\mu} = 10$ MeV. The helium abundance is small except for a narrow region inside the shock wave. All the nuclei are completely dissociated to nucleons after passing through the shock wave because the standing shock is located deep inside the gravitational potential-well in spherically symmetric accretions and, as a result, the post-shock temperature becomes too high for nuclei to survive. There is also a small population of helium ahead of the shock owing to the partial decomposition of nuclei by adiabatic compressions. This small abundance is the main reason why most of the detailed numerical simulations have not incorporated the reactions of neutrino with helium so far. The heating by the inelastic interactions is appreciable only inside the shock wave accordingly. Note also that the value of $Q_{\rm inel}$ is multiplied by a factor of 30 in the figure. It is thus expected that the inelastic reactions will not affect the dynamics at least in the initial phase. This may not be the case for later phases, however. After the non-spherical instability grows, the shock radius becomes larger in general and, as a result, the helium abundance will be increased in a wider region. Moreover, most of these helium will be populated in the so-called heating region (see Fig. 4).

We first summarize the basic feature of the temporal evolution of the reference model L59I0 after 1% of the $\ell = 1$ single-mode velocity perturbation is added. The exponential growth of the perturbation is observed at first and the shock surface is deformed by the increasing amplitude of the non-radial mode. When the non-linear regime is reached, the shock begins to oscillate with a large amplitude. As shown in Fig. 2, where the time evolution of the angle-averaged shock radius is presented, the oscillation becomes quasi-steady by ∼150 ms. Note that the shock radius in this phase is larger than the initial value as pointed by Ohnishi et al. (2006). We have found no shock revival for this model. In fact, as mentioned already, the shock revival is found only for $L_{\nu_e} \geq 6 \times 10^{52}$ ergs s^{-1} if the inelastic interactions are not taken into account. In the last column of Table 1, we summarize for each model if the shock revival is found by ∼500 ms after the onset of computation. It should be noted

that the shock revival, if observed in our models, does not guarantee the explosion in more realistic settings, since the neutrino luminosity will not be constant in time as assumed in our models and will decline in reality. Hence our criterion for the shock revival should be regarded as a minimum requirement for explosion.

Now we proceed to consider the effect of the inelastic interactions of neutrinos with helium. The time evolutions of shock radius for models L59I1, L59I3, and L59I10 are presented in Fig. 2 together with that for the reference model L59I0. These models have the same neutrino luminosity as the reference model and are given the initial velocity perturbation of 1%. The difference is the assumed cross sections for the inelastic reactions. As mentioned earlier, considering the uncertainties that the theoretical estimation inherently has, we multiply the nominal values of the cross sections given by Eqs. (6) and (7), by the factors given in Table 1. Except for model L59I10, the shock oscillations accompanied by the growth of SASI are settled to quasi-steady states by ~ 150 ms just as in the reference model. The final shock radii are not very different from each other among these no-revival models and are larger than that of the initial condition. Model L59I10, whose Q_{inel} is multiplied by a factor of 10, gives a shock revival after a rather long time, ~ 450 ms. As seen in Fig. 2, the evolution in the early phase is essentially the same as for other models, as expected from the helium abundance in the initial condition. This is also seen in the growth rates of the $\ell = 1$ mode presented in Fig. 3. Here we decompose the deformation of the shock surface into the spherical harmonic components;

$$R_{\mathrm{s}}(\theta) = \sum_{\ell=0}^{\infty} a_\ell \sqrt{\frac{2\ell+1}{4\pi}} P_\ell(\cos\theta). \tag{8}$$

Since the system is axisymmetric, only $m = 0$ harmonics, nothing but Legendre polynomials, show up. The coefficients, a_ℓ, can be calculated by the orthogonality of the Legendre polynomials;

$$a_\ell = \frac{2\ell+1}{2} \int_{-1}^{1} R_{\mathrm{s}}(\theta) P_\ell(\cos\theta) d\cos\theta. \tag{9}$$

The position of the shock surface, $R_{\mathrm{s}}(\theta)$, is determined as the iso-entropic surface of $s = 5$. No essential difference can be seen both in the linear phase lasting for ~ 150 ms and the early non-linear phase. Therefore, the additional heating from the inelastic interactions does not play an important role in the growth of SASI.

Figure 4 shows in the meridian section the contours of the mass fractions of nucleons and helium and the neutrino-heating rates for model L59I10. Note that the heating rates for the inelastic reactions (the right half of the right panels of Fig. 4) are plotted in the logarithmic scale whereas those for the others (the left half) are plotted in the linear scale. At 100 ms when the perturbation is still growing in the linear regime, the mass fraction of helium is not

so large in most of the region. One can see some minor heatings via the inelastic interactions both inside and ahead of the shock wave, the latter of which is the preheating considered by Haxton (1988) and Bruenn & Haxton (1991). At 300 ms, however, the shock front wobbles and is deformed substantially by the SASI in the non-linear regime, and a part of the shock reaches larger radii from time to time and the region behind the portion of the shock front contains non-negligible fraction of helium. This is simply because the temperature becomes lower there and nuclei are not completely dissociated. As a result of this increased helium population, the neutrino heating is also enhanced, which then pushes the shock wave further outwards and increases the volume, in which the helium is abundant. This positive feedback finally leads to the shock revival around 500 ms in this model. One can see at this time that most of the region behind the shock contains a large fraction of helium.

We point out here that the shock revival is rather sensitive to the initial amplitude of perturbation as demonstrated in Fig. 5, where we show the evolutions of the angle-averaged shock radius for models L59I0d5, L59I1d5, and L59I3d5. In these models we have imposed 5%, instead of 1%, of the initial velocity perturbation. We can observe that the perturbation grows more rapidly in these models. The non-linear regime is reached in ∼100 ms. More importantly, the shock revival occurs even for model L59I3d5 with the cross sections of the inelastic reactions multiplied by a factor of 3 rather than 10, the value required for the initial perturbation of 1%. Note, however, that the shock revival is achieved without inelastic reactions if we add 10% of velocity perturbation initially (model L59I0d10).

It should be also mentioned that the inelastic interactions lose its importance very quickly as the neutrino luminosity is decreased. As shown in Table 1, the models with $L_{\nu_e} = 5.5 \times 10^{52}$ ergs s^{-1} have not led to the shock revival even if we have multiplied the reaction rates by a factor of 30 (in fact, we have found a factor of 300 is required at least in this model). An interesting thing is that for models with $L_{\nu_e} = 5.8 \times 10^{52}$ ergs s^{-1}, the shock revival has been found for model L58I10 that has a multiplicative factor of 10 whereas the model with the factor of 30 (model L58I30) has not produced a shock revival (see Fig. 6). As shown in Fig. 1, the mass fraction of helium just ahead of the shock is ∼0.2 initially. It seems that the preheating caused by these helium cannot be ignored in this case and, in fact, it tends to suppress the shock oscillations in model L58I30. Although we have ignored the preheating by other nuclei in this paper, they should be taken into account when the critical luminosity is evaluated quantitatively.

Finally we discuss the dependence of the results on the neutrino temperature. As can be understood from Eq. (7), the inelastic scattering rates are very sensitive to the energy of the incident neutrino ($\propto T_\nu^{3.8}$). This naturally leads us to the question what will happen if the energy spectra of neutrinos are harder than commonly assumed. Since higher-

energy neutrinos are more important, here we modify only T_{ν_μ}. The results are given in Table 1 as model L59T-series. Unfortunately, the results are not so sensitive to the neutrino temperature as the cross sections themselves. It is found that for $L_{\nu_e} = 5.9 \times 10^{52}$ ergs s^{-1} the extra heating by the inelastic interactions is large enough to revive the stalled shock only when the temperature of mu and tau neutrinos is higher than $T_{\nu_\mu} = 25$ MeV. This is much larger than the canonical value $\lesssim 10$ MeV and is highly unlikely to be obtained in the supernova core (e.g., Liebendörfer et al. (2001)).

4.   Summary and Discussion

We have investigated the possible effects of the inelastic interactions of neutrino with helium on the shock revival in the post-bounce supernova core. In particular, we have paid attention to their influence on the SASI, one of the major causes for the asymmetry of dynamics and a possible trigger of explosion. For the spherically symmetric models, Bruenn & Haxton (1991) found that both the preheating of matter ahead of the shock and heating of matter behind the shock via these reactions are quite minor. In fact, most of the nuclei are photodisintegrated after passing through the shock and the reactions will scarcely occur anyway in the spherically symmetric models. The situation may be different in non-spherical cases, where the shock wave hovers at larger radius in general and not all the nuclei are dissociated and the heating region is wider. In fact, these reactions have never been explored in the multi-dimensional context so far. We have done 2D numerical experiments on the post-bounce accretion flows through the stalled shock wave onto the protoneutron star, systematically changing the luminosity and temperature of neutrino and the initial amplitude of perturbation as well as the reaction rates.

We have found that the incorporation of the inelastic interactions has essentially no influence on the growth of the SASI, since very little helium is existing in the post-shock matter initially. However, these reactions become appreciable later when the SASI enters the non-linear regime and the shock oscillates with large amplitudes. It has been shown that the extra heating by these interactions is helpful for the shock revival in principle. This is, however, true in practice only when the shock revival is not obtained with a slight margin without the interactions. In fact, we have observed that a small ($\sim 10\%$) reduction of the neutrino luminosity makes the interactions entirely negligible. Hence it is understandable that larger initial amplitudes of perturbation make the interactions more important for shock revival. It is, however, mentioned that even if the luminosity is very close to the critical value, the cross sections estimated by Haxton (1988) seem to be too small. Although it is not easy to evaluate the uncertainties of the theoretical prediction, recent new calculations by Gazit

& Barnea (2004) may be used as a guide. They predicted a bit larger β than Haxton (1988). However, the enhancement of the heating rate for our reference model is only 15%, much too small for the interactions to have some influence on the shock revival. The fact that the dynamics is rather insensitive to the neutrino temperature is not encouraging, either. Hence we conclude that the inelastic interactions of neutrino with helium will be important only in determining the shock-revival-point precisely. It is, however, noted finally that the inelastic neutrino-nuclei interactions should be incorporated in the realistic simulations, since, as we have seen, the preheating may suppress the non-spherical oscillations of the shock wave.

REFERENCES

Ardeljan, N. V., Bisnovatyi-Kogan, G. S., & Moiseenko, S. G. 2005, MNRAS, 359, 333

Blondin, J. M., Mezzacappa, A., & DeMarino, C. 2003, ApJ, 584, 971

Blondin, J. M., & Mezzacappa, A. 2006, ApJ, 642, 401

Bruenn, S. W., & Haxton, W. C. 1991, ApJ, 376, 678

Burrows, A., Hayes, J., & Fryxell, B. A. 1995, ApJ, 450, 830

Burrows, A. & Hayes, J. 1996, Phys. Rev. Lett., 76, 352

Foglizzo, T. 2001, A&A, 368, 311

Foglizzo, T. 2002, A&A, 392, 353

Fryer, C. L. 2004, ApJ, 601, L175

Galletti, P.,& Foglizzo, T. 2005, SF2A-2005: Semaine de l'Astrophysique Francaise, 487

Gazit, D., & Barnea, N. 2004, Phys. Rev. C, 70, 048801

Haxton, W. C. 1988, Phys. Rev. Lett., 60, 1999

Houck, J. C., & Chevalier, R. A. 1992, ApJ, 395, 592

Herant, M., Benz, W., Hix, W. R., Fryer, C. L., & Colgate, S. A. 1994, ApJ, 435, 339

Janka, H.-T., & Mueller, E. 1996, A&A, 306, 167

Janka, H.-T., Buras, R., Kitaura Joyanes, F. S., Marek, A., Rampp, M., & Scheck, L. 2005, Nucl. Phys. A, 758, 19

Kifonidis, K., Plewa, T., Scheck, L., Janka, H.-Th., & Mueller, E. 2005, A&A, in press (astro-ph/0511369)

Kotake, K., Sawai, H., Yamada, S., & Sato, K. 2004, ApJ, 608, 391

Kotake, K., Sato, K., & Takahashi, K. 2006, Rept. Prog. Phys., 69, 971

Liebendörfer, M., Mezzacappa, A., Thielemann, F.-K., Messer, O. E., Hix, W. R., & Bruenn, S. W. 2001, Phys. Rev. D, 63, 103004

Ohnishi, N., Kotake, K., & Yamada, S. 2006, ApJ, 641, 1018

Sawai, H., Kotake, K., & Yamada, S. 2005, ApJ, 631, 446

Scheck, L., Plewa, T., Janka, H.-T., Kifonidis, K., & Müller, E. 2004, Phys. Rev. Lett., 92, 011103

Shen, H., Toki, H., Oyamatsu, K., & Sumiyoshi, K. 1998, Nucl. Phys. A, 637, 435

Stone, J. M. & Norman, M. L. 1992, ApJS, 80, 753

Takiwaki, T., Kotake, K., Nagataki, S., & Sato, K. 2004, ApJ, 616, 1086

Wang, L., Wheeler, J. C., Li, Z., & Clocchiatti, A. 1996, ApJ, 467, 435

Wang, L., Howell, D. A., Höflich, P., & Wheeler, J. C. 2001, ApJ, 550, 1030

Wang, L., et al. 2002, ApJ, 579, 671

Yamada, S., & Sawai, H. 2004, ApJ, 608, 907

Yamasaki, T., & Yamada, S. 2005, ApJ, 623, 1000

Yamasaki, T., & Yamada, S. 2006, submitted to ApJ

Yamasaki, T., & Yamada, S. 2006, in preparation

Table 1.   Model Parameters

Model	L_{ν_e} (10^{52} ergs s^{-1})	Q_{inel} (Eq. (6))	$\delta v_r/v_r^{1D}$ (%)	$T_{\nu_{\mu,\tau}}$ (MeV)	Shock Revival
L59I0	5.9	–	1	10	X
L59I1	5.9	×1	1	10	X
L59I3	5.9	×3	1	10	X
L59I10	5.9	×10	1	10	◯
L59I30	5.9	×30	1	10	◯
L59I0d5	5.9	–	5	10	X
L59I1d5	5.9	×1	5	10	X
L59I3d5	5.9	×3	5	10	◯
L59I0d10	5.9	–	10	10	◯
L59T15	5.9	×1	1	15	X
L59T20	5.9	×1	1	20	X
L59T25	5.9	×1	1	25	◯
L58I0	5.8	–	1	10	X
L58I1	5.8	×1	1	10	X
L58I10	5.8	×10	1	10	◯
L58I30	5.8	×30	1	10	X
L55I0	5.5	–	1	10	X
L55I1	5.5	×1	1	10	X
L55I10	5.5	×10	1	10	X
L55I30	5.5	×30	1	10	X

Note. — L_{ν_e} represents the luminosity of electron-type neutrino. For Q_{inel}, only the multiplicative factor is given. $\delta v_r/v_r^{1D}$ denotes the initial relative amplitude of velocity perturbation in percentage. $T_{\nu_{\mu,\tau}}$ is the temperature of mu and tau neutrinos. The "successful shock revival" is defined as a continuous increase of the shock radius by $\sim$500 ms.
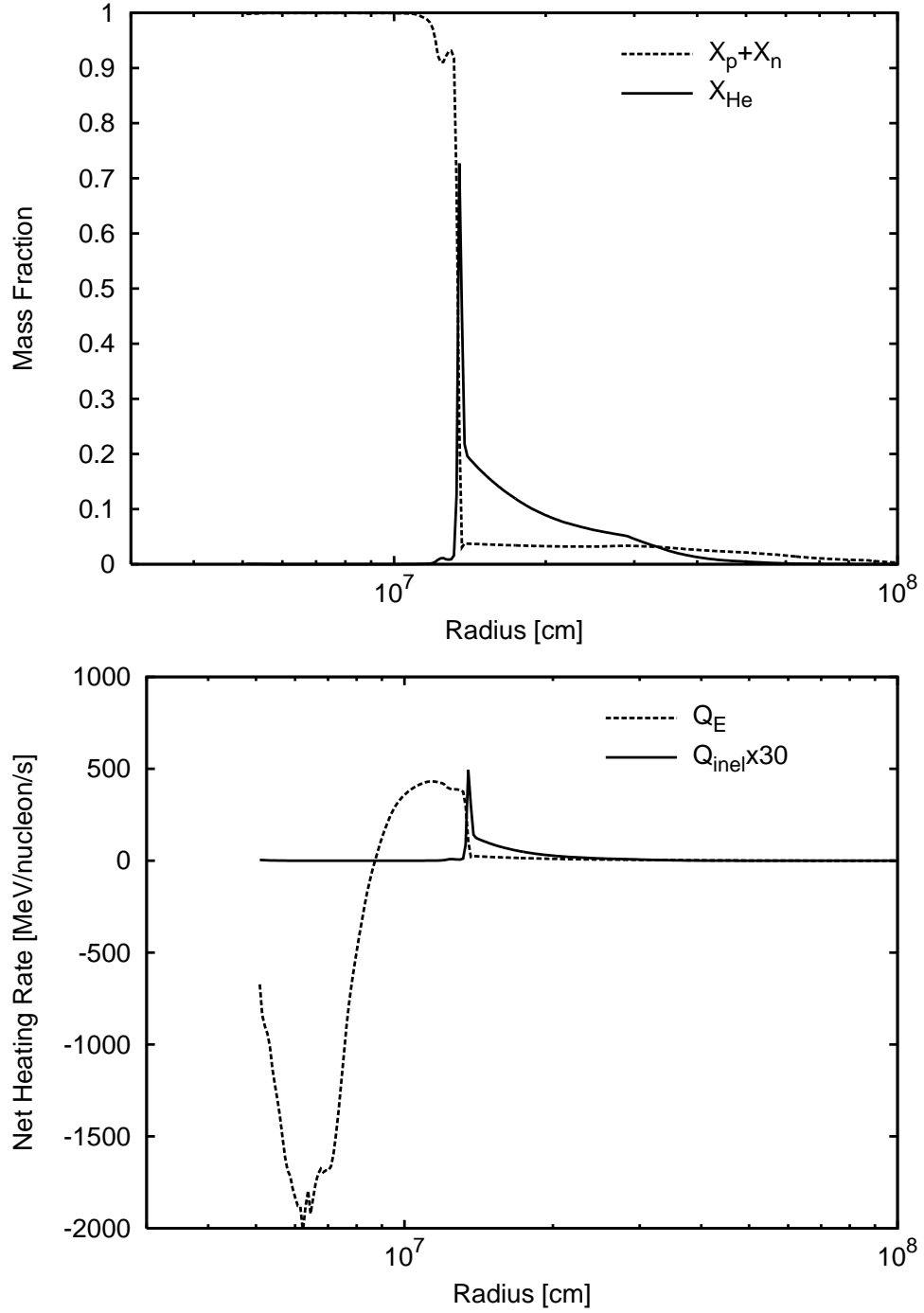
Fig. 1.— The mass fractions of helium and nucleons (upper panel) and the heating rates (lower panel) at the initial time for the reference model L59I0. The solid and dashed lines in the upper panel denote the mass fractions of helium and nucleons, respectively. The lower panel represents the net heating rates by absorptions and emissions on nucleons (solid line) and the inelastic interactions with helium (dashed line). Note that the latter rate is multiplied by a factor of 30.
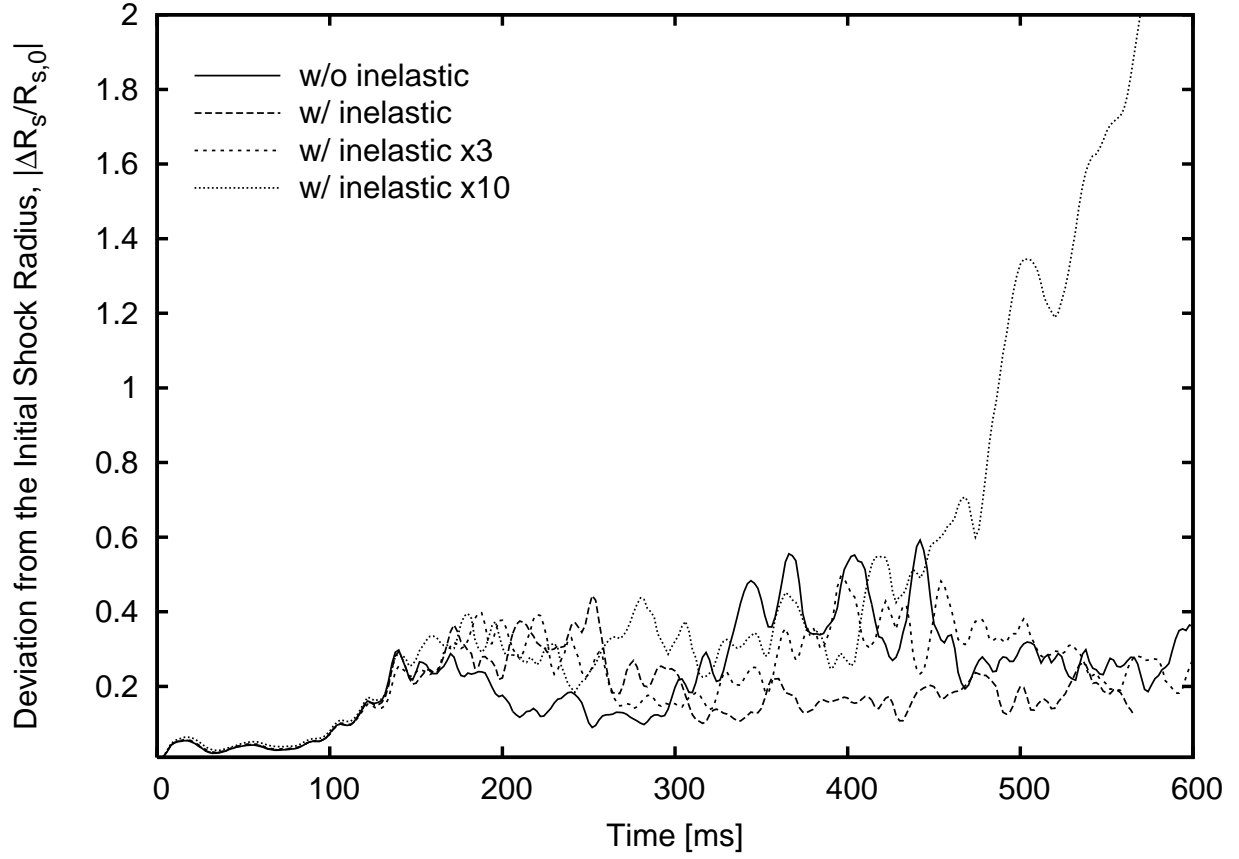
Fig. 2.— The temporal evolutions of the angle-averaged shock radius for the models with $L_{\nu_{\mathrm{e}}} = 5.9 \times 10^{52}$ ergs s^{-1}. The relative deviations from the initial value are plotted for models of L59I0, L59I1, L59I3, and L59I10.
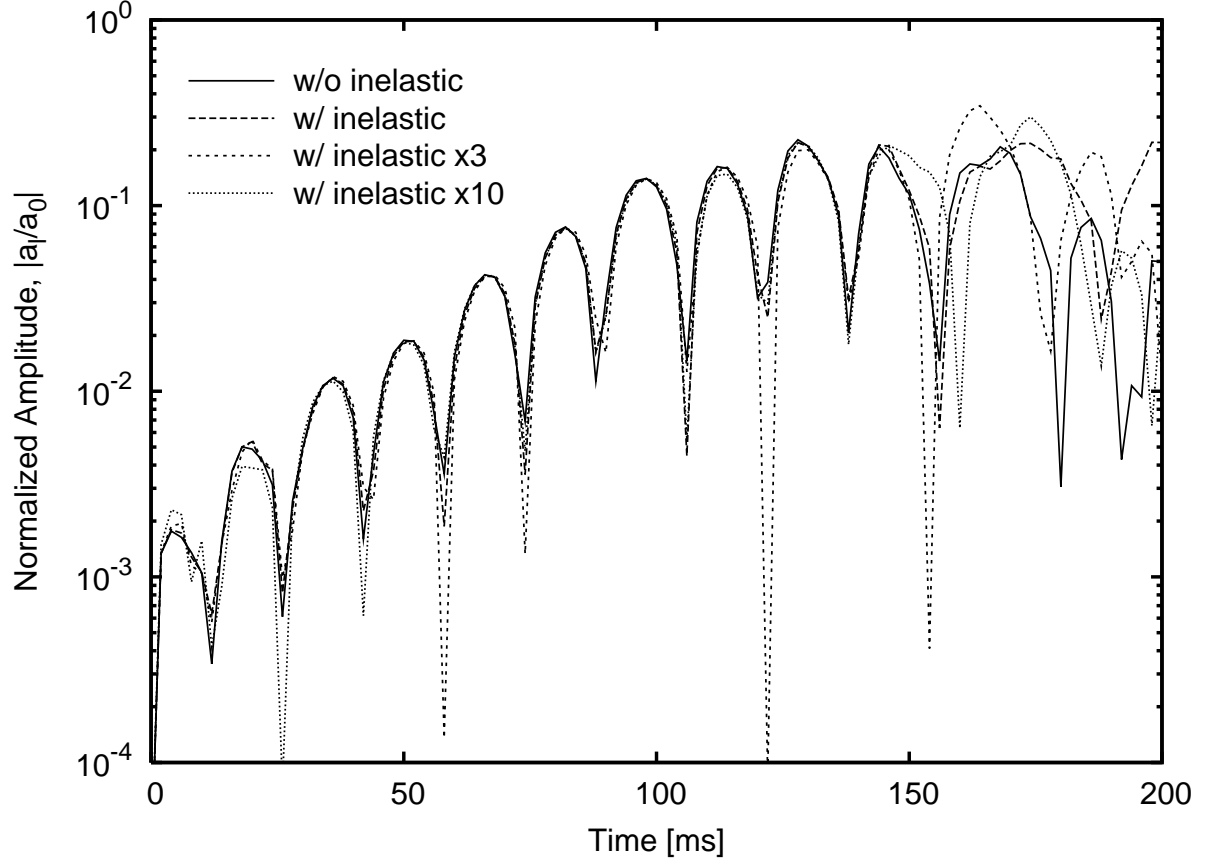
Fig. 3.— The temporal evolutions of the normalized amplitudes of the $\ell = 1$ mode in the spherical harmonic decompositions for models L59I0, L59I1, L59I3 and L59I10. See the text for details.
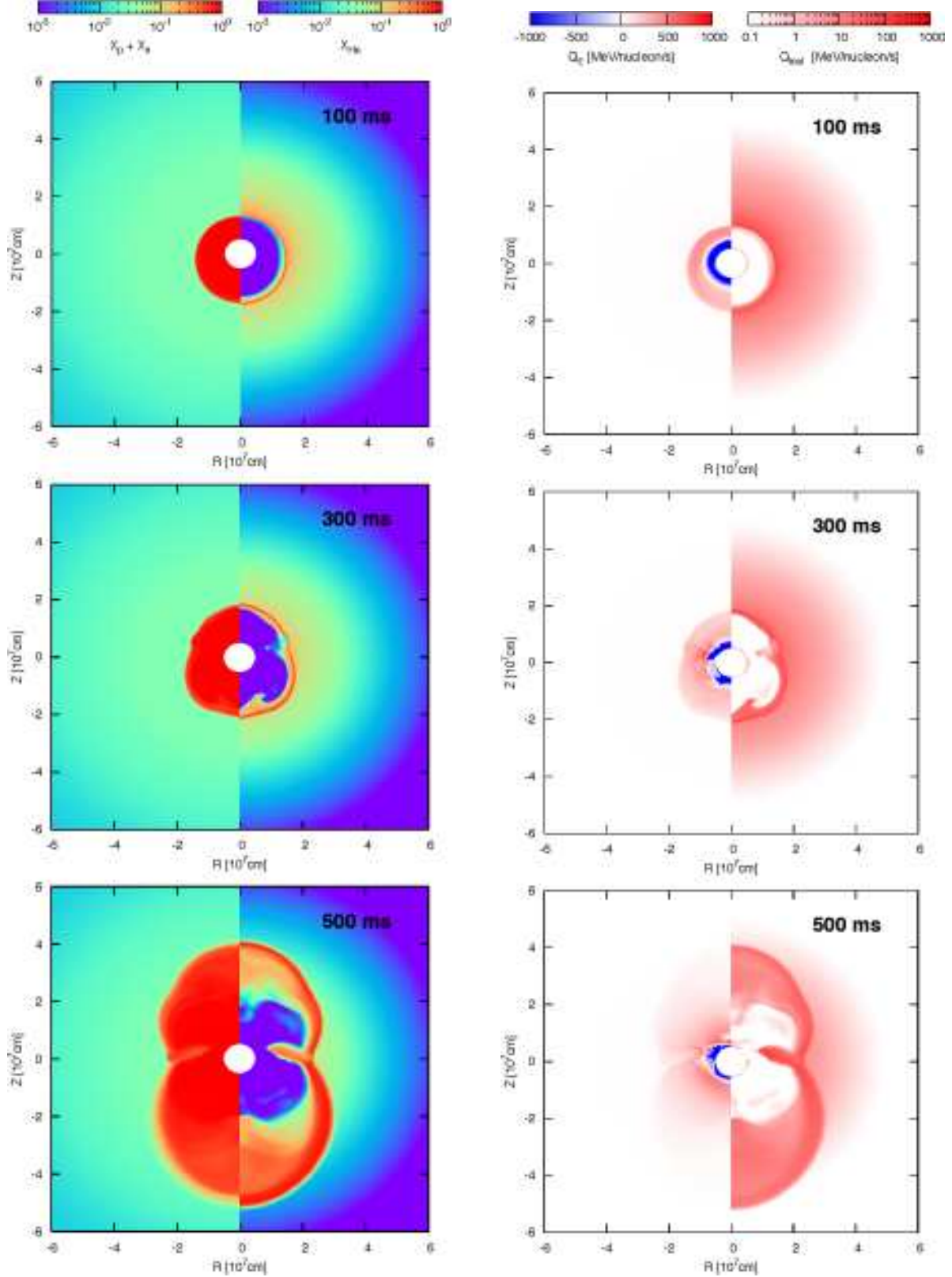
Fig. 4.— The contours in the meridian section of the mass fractions (left panels) and net heating rates (right panels) for model of L59I10. The left and right halves of each left panel represent the fractions of nucleons and helium, respectively. The heating rates are plotted for the neutrino-nucleon reactions (left half) and the inelastic interactions of neutrino with
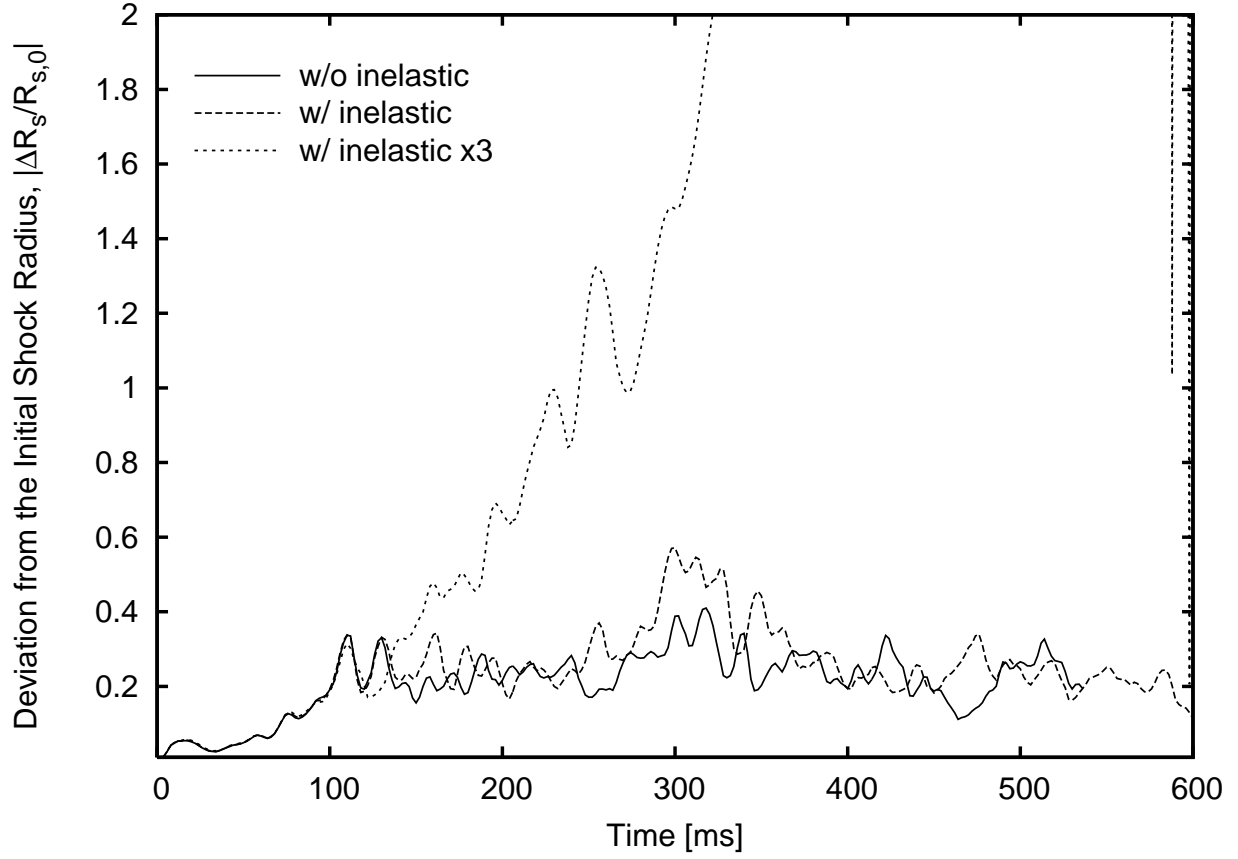
Fig. 5.— The temporal evolutions of the angle-averaged shock radius for the models with 5% of initial velocity perturbation ($L_{\nu_e} = 5.9 \times 10^{52}$ ergs s^{-1}). The relative deviations from the initial value are plotted for models L59I0d5, L59I1d5, and L59I3d5.
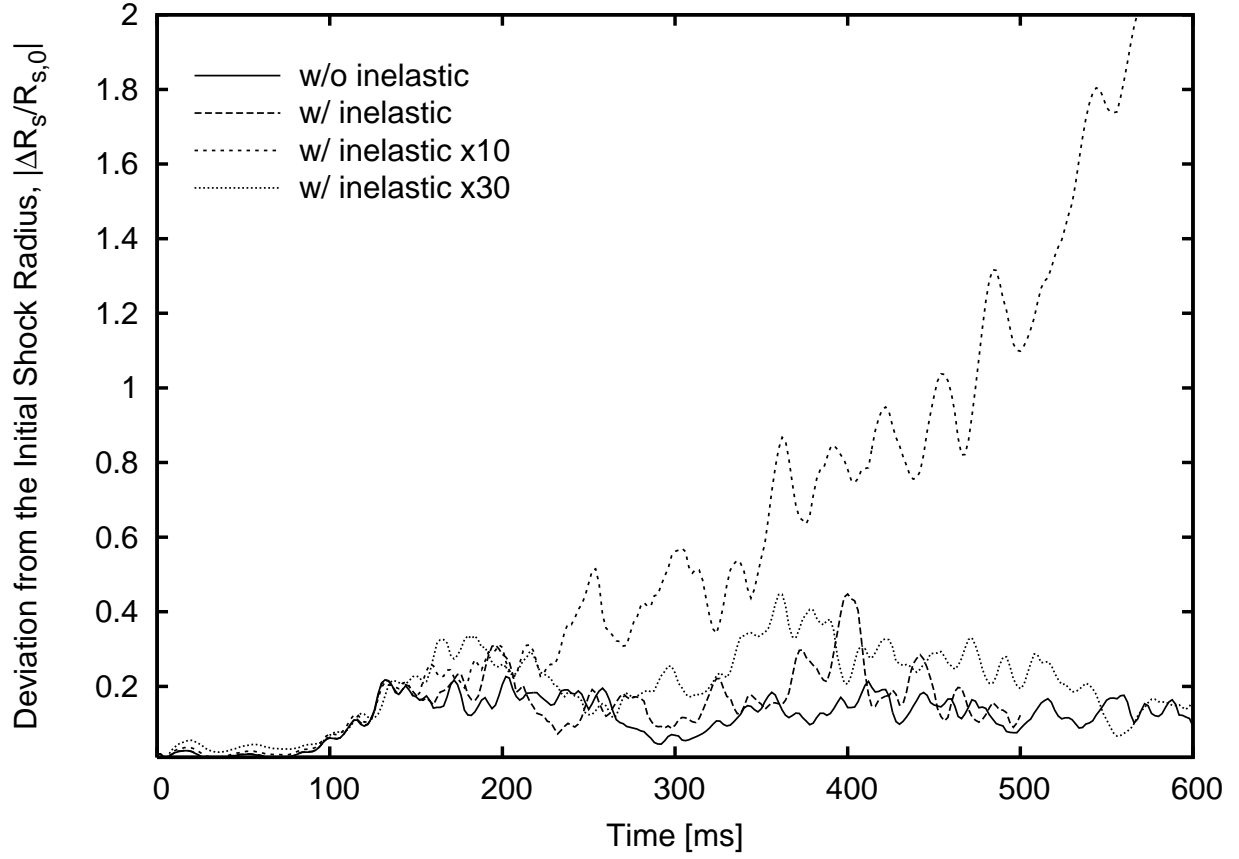
Fig. 6.— The temporal evolutions of the angle-averaged shock radius for the models with $L_{\nu_e} = 5.8 \times 10^{52}$ ergs s^{-1}. The relative deviations from the initial value are plotted for models L58I0, L58I1, L58I10, and L58I30.